Shweta and Jha *Bioresour. Bioprocess.* (2016) 3:31
DOI 10.1186/s40643-016-0107-7

Bioresources and Bioprocessing

RESEARCH Open Access

Synthesis and characterization of crystalline carboxymethylated lignin–TEOS nanocomposites for metal adsorption and antibacterial activity

Kumari Shweta and Harit Jha*

Abstract

Biodegradable carboxymethylated lignin–tetra ethoxysilane (TEOS) nanocomposites (CML–T) were synthesized using lignin extracted from rice straw (RS) followed by surface modification through carboxymethylation. Composites were characterized by UV-spectroscopy, Fourier transform infrared (FT-IR), scanning electron microscope (SEM), X-ray diffraction pattern (XRD), atomic absorption spectroscopy (AAS) and particle size distribution (PSD). The average diameter (D_{50}) of the CML–T composite particles was observed in the range of 160–560 nm. XRD spectra and SEM micrographs confirmed the high degree of crystallinity (peaks located at lower angle, $2\theta = 12$ and 22.0°) and porous nature of nanocomposites with increasing concentrations of TEOS. The composite exhibited nickel (Ni^{2+}) and cadmium (Cd^{2+}) adsorption up to 70.72 and 81.79 %, respectively in AAS analysis. The CML–T composite was investigated to assess their future applications as wound dressings and antimicrobial and packaging agents. Based on the antimicrobial properties and potential to remediate toxic heavy metals, the composites are proposed to be used for wastewater treatments, as packaging materials and for preparation of biofilters for environmental protection.

Keywords: Lignocellulose wastes, Sol–gel mechanism, Composites, Crystallinity, Adsorption, Antimicrobial agent

Background

Agricultural wastes owing to low natural degradation rate hinder the carbon cycle and are commonly eliminated by incineration, leading to pollution. Agricultural waste materials, however, are good sources of low-cost adsorbents and value-added product obtained through physico-chemical modifications (Paul and Robeson 2008). A number of biodegradable biocomposites and biofilms have been prepared from natural mixtures (carbohydrates, proteins, lipids, and fibres) obtained in the flour form of raw materials of plant origin, such as cereals, tubers and rhizomes (Maniglia et al. 2014). The natural, renewable, biodegradable and biocompatible polymers have been used for applications such as remediation of industrial effluents (Kumar et al. 2015) and in the medical (Reis and Gomes 2004) field (used in tissue engineering for preparing scaffolds). They are preferred due to their good biocompatibility and mechanical properties similar to those of hard and soft tissues and easy fabrication into a variety of shapes with adjustable interconnecting porosity (Slavutskya and Bertuzzi 2014). When compared to pure polymers, polymer nanocomposites possess many attractive properties, such as enhanced barrier characteristics, increased moduli and strengths, high heat distortion temperatures, reduced gas permeability and decreased absorption in organic liquids (Gulyas et al. 2013). Rice straw (RS), one of the most widely available agricultural wastes, has an annual production of over 600 million tons (Zhang et al. 2010). The hard surface, small bulk density and high amorphous silica content make RS suitable for the synthesis of biopolymer-based biomaterials having wider applications in environmental remediation and therapy (Gupta et al. 2016).

*Correspondence: harit74@yahoo.co.in
Department of Biotechnology, Guru Ghasidas Vishwavidyalaya (A Central University), Bilaspur, Chattisgarh 495009, India

Industrial effluents are the major sources of heavy metal contamination of water resources. Nickel, arsenic and cadmium are some of the toxic pollutants present in wastewater for electroplating, battery, mining and metallurgy, aircraft, pigments and ceramic industries (Salem and Awwad 2011). Bioaccumulation of these heavy metals in the food chain causes serious health hazards and disorders to all the biotic components of the ecosystem, including human beings. Cadmium toxicity results in a wide range of syndromes including renal dysfunction, hypertension, hepatic injury, lung damage and teratogenic effects. Excessive exposure to nickel can significantly increase the risk of lung, cardiovascular and kidney diseases in humans (Heidari et al. 2013). Chromium (Cr), cadmium (Cd) and nickel (Ni) compounds are also widely used in industries, such as leather tanning, electroplating, metal finishing, paint and pigments, and therefore discharge of these metals in large quantities into industrial effluents cannot be ruled out. Water containing a high concentration of these metals can cause serious environmental problems as well as induce toxic and carcinogenic health effects on humans. Therefore, the removal or minimizing the toxicity of the metal ions from wastewaters has been a matter of great concern.

Major methods that have been used to remove metal ions from wastewater include adsorption, chemical precipitation, ion exchange, electrolytic extraction and membrane filtration, yet most of them have disadvantages like high cost, large input of chemicals and incomplete removal. Effective treatment of wastewater containing these environmental pollutants has become a challenging task due to the cost of the treatment and, thus, demanding the development of new alternative cost-effective methods (Li et al. 2012).

A number of raw lignocellulose-based adsorbents have potent metal adsorption capacity (Sciban et al. 2014). Recent studies by several research groups have indicated that RS and agave bagasse have higher adsorption capacity for nickel, cadmium and chromium compared to sorghum or oat straw (Li et al. 2012). The concentration of binding sites in RS polymers could be increased, based on the facts that the natural adsorption capacity of some lignocellulosic materials may be improved with chemical treatments and surface modifications with basic solutions, minerals and organic acids, organic compounds and some oxidizing agents (Mendez et al. 2013).

The present work was undertaken with the aim of preparing inexpensive, effective, crystalline and porous lignin–TEOS based composites using lignin extracted from the RS, which could be an alternate source for treatment of environmental pollutants. The nanocomposite materials thus synthesized were characterized and their potential in industrial waste treatment was assessed by UV spectrum, FT-IR, SEM, XRD, AAS and PSD analyses. The approach was to replace the existing commercial lignin with extracted lignin, followed by chemical surface modification to synthesize biocompatible and biodegradable nanocomposites. Additionally, the antimicrobial activities against various microbial contaminants make them applicable as packaging materials for enhancing the shelf life of food stuffs.

Methods

Extraction of lignin from RS and surface modification through carboxymethylation

RS was collected from the rice mill of Bilaspur (C.G.) in India. The extraction of lignin from RS was performed using hot water by the method described earlier (Shweta and Jha 2015).

Surface treatment of lignin was performed as described by the method of Yadav et al. (2014) with minor modifications. In brief, 100 mg of hot water-extracted lignin (HL) was mixed with 72 % ethanol and continuously stirred for 30 min at 25 °C, followed by dropwise addition of NaOH (30 %, w/v) to this mixture. After shaking for 90 min, 15 mL of acetic acid was added and the resulting mixture was stirred for 3.5 h at 55 °C. The solution thus obtained was filtered and suspended in 95 % ethanol and neutralized with acetic acid. The final product was washed thrice with 95 % ethanol and the anionic sodium carboxymethylated lignin (CML) was dried overnight at 60 °C for further use in the synthesis of composite material.

Synthesis of CML–T nanocomposites using TEOS

CML–T composites were synthesized as described by the method described previously (Yang et al. 2014) with minor modifications. Initially, lignin was dissolved in 5 % (w/v) NaOH (pH = 13.0) in 1:1 ratio and subsequently heated at 70 and 95 °C for 1 h each. Different concentrations of TEOS (1, 2 and 3 %) were mixed in the solution with vigorous shaking at 300 rpm. The pH of the solution was adjusted to 6.0 with slow stirring for 3 h to form a gel in the presence of TEOS with aggregation of the mixture. The gel was filtered with Whatman filter paper (Grade: 42) with retention capacity of 1.5 μm and filtration rate at 4 mL/min. The gel was completely dried in cold at 4 °C for 1 week. Dried CML–T composites were crushed and stored in airtight glass vials used for further physicochemical analyses. An alkaline solution of CML without TEOS was used as the control.

Spectral study of CML–T nanocomposites

The synthesized composites and the control samples were initially crushed in a mortar and pestle, dissolved in preheated deionized water (1:2, w/v) and sonicated using ultrasonic homogenizer (Biologics Inc. 3000) at 40 W

with 60 % pulse rate for 30 min. The processed samples were then subjected to spectral analyses (Nassar and Youssef 2012).

FT-IR analysis

Unmodified (extracted lignin), surface-modified lignin (CML) and dried CML–T composite samples were separately mixed with KBr at a concentration of 1/100 mg KBr (w/w) for FT-IR analysis. The spectra were taken in absorption mode in the range of 400–4000 cm^{-1} with a resolution of 8 cm^{-1} and 32 scans in an FT-IR spectrophotometer (Thermo Nicolet model Avtar 370 G) as described recently (Kim et al. 2014).

Particle size analysis (PSD)

The particle size of the CML–T composites was determined by a laser diffraction apparatus (Malvern Instruments Ltd, Zetasizer version 6.2, UK). Samples were dissolved in preheated deionized water (1:2, w/v) and sonicated at 40 W with 60 % pulse rate for 30 min (Abdel-Halim et al. 2009). To improve the sample dispersion, 80 % ethanol was used as the solvent. The surface charge and size of the composites were analysed using light scattering at room temperature (25 ± 2 °C) in triplicate and the results were presented as the mean value ± S.D.

X-ray diffraction (XRD)

Crystallinity of the samples (CML–T composites) was determined by X-ray diffraction (XRD) using X-ray diffractometer (PAN analytical 3KW X'pert powder, multifunctional). The X-ray was energized by 45 kV and 10 mA. The step-scan mode was 0.1° 2θ and the time of scan 1 s; 2θ ranged from 20 to 80° (Zhang et al. 2011).

Crystallinity index (I_{cr} %)

The crystallinity index (I_{cr} %) of the CML–T composites was calculated using (1), following the method proposed by Segal et al. (1959).

$$\frac{I_{\mathrm{Cr}} = I_{200} - I_{\mathrm{am}}}{I_{200}} \times 100, \tag{1}$$

where I_{200} is the diffraction intensity close to $2\theta = 22$–24°, which represents a crystalline structure of a material; I_{am} is the diffraction intensity close to $2\theta = 18°$, which refers to the amorphous structure of the material.

Grain size

The diffraction patterns for the prepared CML–T composites were recorded on X-ray diffractometer equipped with Cu–Kα radiation ($\lambda = 0.154$ nM) with a scan rate of 0.02°S^{-1}. The average particle size of composites was determined using Debey–Scherrer's equation (Eq. 2) (Alexander and Klug 1949 and 1950) as follows:

$$\text{Grain size } (D) = \frac{0.9\lambda}{\beta cos\theta}, \tag{2}$$

where D is the grain diameter (nm), β the FWHM (full width at half maxima), θ the diffraction angle in radian and λ the X-ray wavelength (1.54 Å or 0.1541 nm).

Porosity (%)

The porosity of the prepared CML–T composites was recorded on an X-ray diffractometer using Eq. (3) (Shilin et al. 2012),

$$P = [1 - (n2 - 1/nT2 - 1)] \times 100\,(\%), \tag{3}$$

where P is the porosity of the material, n_T the refractive index of the material and n the calculated value of the material.

Study of electrical conductivity, turbidity, effect of CML–T composites on soil and estimation of organic matters in nanocomposites

0.5 g of lignosulphonate, TEOS and composites were thoroughly mixed mechanically with a magnetic stirrer in a ultrasonic bath in 50 mL of deionized water for 1 h for breaking agglomerates at RT in the electric field with intensity ~100 V/m (Ichkitidze et al. 2013). Further electrical conductivity was measured by conductivity meter 304 (Systronics).

The turbidity could be determined by the clarity of the solution after mixing 0.5 g each of the control and test samples in 20 mL of deionized water (Snowden et al. 2012).

The basic properties that can influence the behaviour of nanocomposites, i.e. texture, organic carbon, pH and electrical conductivity, were determined on the basis of soil fraction according to the standard procedure reported in the Methods of Soil Analysis (SSSA Book Series, Methods in Soil Analysis 1996). Soil sample was collected from the top layer (0–15 cm) of a local agricultural field in Bilaspur (C.G.). Initially, the soil sample was air dried and sieved through a 2 mm sieve to remove grasses, pebbles and stones. Further, it was homogenized using mortar–pestle. 5 g of pre-weighed soil sample was taken in six different flasks. 0.5 g of lignosulphonate, TEOS, CML–1T, CML–2T and CML–3T were mixed in each flask, dissolved in 50 mL of deionized water and kept for continuous shaking at RT for 24 h for soil analysis. The flask containing only the soil sample was taken as the control.

The content of organic matters in CML–T composites was estimated by Lowry's method (for protein estimation), anthrone test (for carbohydrate estimation) and lipid estimation test (Sadasivam and Manickam 2008).

Scanning electron microscopy (SEM)

The surface morphology of the CML–T composites was visualized using an SEM (Zeiss) with an operating voltage at 10 kV. Images were taken at different magnifications as described earlier (Malarvizhi et al. 2014).

Antimicrobial test

Well diffusion method (Nassar and Youssef 2012) was performed to determine the antimicrobial properties of the composites. The test microorganisms (Gram negative: *Pseudomonas aeruginosa* MTCC 741, *Escherichia coli* MTCC 739 and Gram positive*: Bacillus subtilis* MTCC 441 and *Staphylococcus aureus* MTCC 96 were spread over nutrient agar (NAM) plates. The well in the centre of the culture plates (pre-incubated at 28 ± 2 °C) was loaded with aqueous suspension containing different concentrations (10, 20, 30 and 40 µL) of CML–T composites prepared in sterile deionized water. The plates were further incubated at 28 ± 2 °C for 24 h and the diameter of the inhibition zone surrounding the well was subsequently measured with a ruler up to 1 mm resolution. The experiments were performed in triplicate and the results were expressed as mean ± SD.

Metal adsorption

Procedure

Aqueous solutions of Cd (II) and Ni (II) ions for the batchwise experiments were prepared in a buffer solution (0.1 M HNO_3 and 0.1 M HEPES [(N-[2-hydroxy ethyl] piperazine-N′-N-[ethane sulphonic acid])], pH 3.0. The pH of the buffer solution was adjusted with 0.1 M NaOH in the range of 1.0–5.0 for further experimentation. CML–T composites (20, 40 and 60 mg/L) were mixed with 25 mL each of metal solution (0.1 M) and kept for vigorous shaking at ambient temperature (25 + 2 °C) for different time intervals (0, 24, 48 and 72 h). The effects of the initial concentrations of nickel and cadmium ions on adsorption were studied by varying their concentrations at a constant pH value (Parajuli et al. 2005).

Adsorption kinetics

Determination of nickel and cadmium biosorption by AAS analysis

Study of the biosorption efficiency and kinetics of biosorbents was conducted under static conditions employing a glass vessel equipped with a rotary shaker. The adsorbent CML–T composites (20, 40 and 60 mg/L) were incubated under shaking conditions (120 rpm) with 100 mL of 0.1 M solutions of nickel and cadmium. The concentration of Ni (II) and Cd (II) ions in the solution was determined at fixed intervals by AAS analysis (atomic absorption spectrophotometer, SL-173, Shimadzu). The amount of Ni (II) and Cd (II) ions adsorbed, qt (mg/g) at different time intervals, was calculated as described in Eq. (4) (Salem and Awwad 2011).

Metal solutions were acid digested and subjected to AAS analysis for determination of total dissolved metal. The test samples were digested in a 1:1 ratio of aqua-regia. Subsequently, samples were kept under vigorous shaking for 24 h at ambient temperature followed by filtration (Whatman filter paper Grade 42 with retention capacity of 1.5 µm and filtration speed rapidity at 4 mL/min). The filtrates were collected in glass vials for AAS analysis (Nardis et al. 2004).

The initial and final concentrations of heavy metal ions were determined in the sample solutions. The amount of heavy metal ions adsorbed per specified amount of adsorbent (q) (4) and adsorption efficiency (5) were calculated as follows (Heidari et al. 2013):

$$q = \frac{(\mathrm{Co}-\mathrm{Ce})v}{w}, \tag{4}$$

$$\%R = \frac{(\mathrm{Co}-\mathrm{Ce})}{\mathrm{Co}} \times 100, \tag{5}$$

where q (mg/g) is the amount (mg) of metal ions adsorbed per mg of adsorbent (adsorption capacity), Co (mg/L) the initial concentration of metal ions, Ce (mg/L) the final concentration of metal ions, v (mL) the volume of metal solution and w (g) the weight of the adsorbent.

Statistical analyses

All the experiments were performed in triplicate. The yield obtained for CML–T composites was statistically analysed and their mean ± S.D. was determined. Analysis of average, standard deviation and standard error was performed using Graph Pad Prism 5.

Results and observations

Synthesis of carboxymethylated lignin–TEOS composites and their spectral study

Hot water-extracted lignin from RS was subjected to surface modification by carboxymethylation to obtain free functional groups to increase the binding efficiency (Kumagaia and Matsuo 2013). A higher percentage of CML could be achieved only if the reactivity of the extracted lignin was chemically enhanced, and one of the reactivity-enhancing processes used in our study was carboxymethylation for hybrid synthesis as described earlier (Atwood and Lehn 1996). Previous reports suggested that the lignin yield was dependent on the solvent used (Zhang et al. 2010). Increase in the concentration of alkali might reduce the complexity and molecular size of modified lignin and disrupt the chemical bonds present in lignin, cellulose and hemicelluloses. The carbonium ions in the resulting intermediates react with an electron-rich

carbon to form stable carbon–carbon linkages, leading to condensation of lignin (Wang et al. 2013).

Sol–gel mechanism is one of the best methods (Yang et al. 2007) to synthesize biocomposites based on lignocellulosic waste material (RS). During synthesis of CML–T composites, it was observed that with the increasing concentration of TEOS, the yield of the hybrid (CML–T composite) also increased proportionately in comparison to the control (without TEOS), possibly due to the increased interaction between organic and inorganic phases resulting in a high degree of agglomeration for gel formation during sol–gel reaction. The yields of control, CML–1T, CML–2T and CML–3T obtained were 12.12 ± 0.10, 14.95 ± 0.12, 20.11 ± 0.11 and 14.48 ± 0.06 % (w/w), respectively. Results showed that the physico-chemical parameters used in the experiment were suitable to prepare the composite. Specific characteristics of these composites have been represented in Table 1. The λ_{max} of CML–1T, CML–2T, CML–3T, control (reaction mixture without TEOS) and TEOS were observed at 350, 420, 420, 480 and 415 nm, respectively. High intense peaks at 420 nm were observed for CML–2T and CML–3T, probably due to the electronic transition of non-conjugated aromatic ring as described earlier (Mohamed et al. 2013). Solution mixtures of carboxymethylated lignin turned dark brown after 3 h of chemical reaction in the presence of TEOS due to the subsequent hydrolysis and condensation (sol–gel) reactions between hydroxyl groups of lignin to form siloxane bonds. The colour of composites and intensity of the spectral peaks were concentration dependent on the silane group of TEOS. The results indicated that without TEOS, hydrolysis and condensation reactions could not take place under the reaction conditions. With the increase in the concentration of TEOS (1, 2 and 3 %), colour change was observed from light brown to dark brown (Fig. 1).

The FT-IR spectra of the samples recorded in the range of 400–4000 cm^{-1} were used to examine the surface groups of lignin and CML–T composites and to identify the groups responsible for the synthesis of CML–T composites. The peaks thus obtained (Fig. 2a) might be due to plasmon resonance. As previously discussed, a change in the colour was observed due to synthesis of CML–T composites; a characteristic peak of composite in the range of 2000–3000 nm^{-1} in the FT-IR spectra further validated the observations (Tibolla et al. 2014). The intense peaks of extracted lignin and carboxymethylated lignin were found in the range of 2000–3500 cm^{-1} (Fig. 2a). FT-IR results indicated that the interaction of chemical bonds of methyl and carboxyl groups occurred with the O–H bonds of phenols and alcohols present in the lignin structure, because these groups undergo a shift to lower wavenumbers after synthesis of the silanol (Si–OH) group. During composite synthesis, the hydrolysis reaction of silane leads to the substitution of the –OH groups on the surface of lignin and the resulting Si–OH group helps in condensation reaction with the organic component. The reaction between two different phases leads to the formation of a stable bond and thus releases free alcohol as a by-product, resulting in the formation of lignin polyol derivatives, which in turn improves the solubility of lignin. With the increasing concentration of TEOS, the intensity of peaks also changed without affecting their position (Fig. 2b), as reported previously (Lin et al. 2014). The peak positions of various modes of vibrations in the FT-IR spectra of lignin, carboxymethylated lignin and CML–T composites during sol–gel reaction are represented in Table 2.

The additive (TEOS) has been reported to increases the crystallinity of the prepared composite material (Gardebjer et al. 2014). As such, the surface morphological properties of the CML–T nanocomposites containing different concentrations of TEOS (1, 2 and 3 %) were examined by SEM (Fig. 3). Porous areas with oval and circular pores were observed at higher concentrations of TEOS. Further increase in the concentration of TEOS leads to relatively homogenous dispersion of silica microparticles within the matrix. The number and size of silica microparticles also increases with the increase in concentration of TEOS (Gao et al. 2009). This may play an important role in the formation of triangle crystalline arrangement of nanocomposites as explained in the later part of the result (XRD). Moreover, the silica microparticles dispersed in the matrix could form crystalline and porous segments in the hybrids that offered a large surface area in the polymer for chemical and physical interactions for various applications such as adsorption of environmental pollutants (like heavy metals, dyes, etc.) and antimicrobial activity.

Table 1 Characteristics of the retained CML–T composites

S. No.	Composite name	Visual appearance	Appearance of shape under scanning electron microscopy	Size (in nm)	% Removal efficiency	Antimicrobial activity
1	CML–1T	White	Crystalline	65.89 ± 2.37	58.19 ± 0.94	Positive
2	CML–2T	Light brown	Irregular	56.00 ± 0.96	81.79 ± 1.89	Positive
3	CML–3T	Dark brown	Oval	16.00 ± 0.36	70.72 ± 1.67	Negative

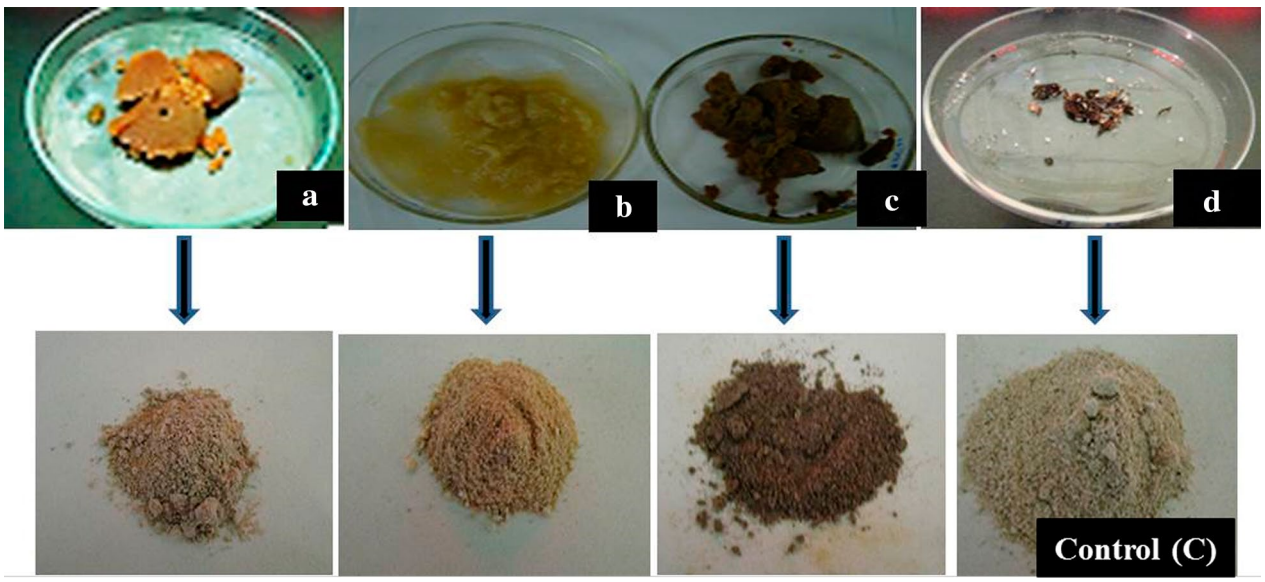

Fig. 1 Visual observation of carboxymethylated lignin–TEOS (CML–T) composites on the basis of increasing concentration of TEOS: **a** CML–1T (1:1), **b** CML–2T (1:2), **c** CML–3T (1:3), **d** control (C or CML without TEOS)

The particle size distribution (PSD) curves (Stober et al. 1968) of the CML–T composites showed the average particle size (D_{50}) for CML–1T, CML–2T and CML–3T as 120, 100 and 160 nm, respectively (Fig. 4). The viscosity (Cp) was found to be 0.1000 (with accuracy of ±1 %) for all the three samples. It seems most probable that TEOS had reduced the surface energy and the electrostatic forces in the composites, thereby samples were deagglomerated. There was no increase in the particle diameter after surface modification, as in the case with silane coupling agents (Gao et al. 2009) such as TEOS. SEM images corroborated an irregular morphology with crystalline structures with size ranging from 100 to 160 nm. The smaller size and irregular morphology might provide additional surface area for adsorption of metal ions and interaction with microorganisms.

The XRD patterns demonstrated the crystalline structure of CML–T nanocomposites. The basal spacing reflections of the composites indicate a sharp peak at $2\theta = 12.20°$, which translates to a basal spacing of 7.35A°. The presence of basal reflection at $2\theta = 24.50°$ is an evidence of dehydration. The XRD profiles of lignin-based composites are shown in Fig. 5. In appearance, characteristic diffraction angles were displayed at $2\theta = 12°$ corresponding to the (1.10) plane, while the peak at $2\theta = 20.0°$ and 22.0° corresponded to (110) and (020) planes, respectively. The peaks correspond to the crystalline structure of CML–T composites (Hanid et al. 2014). Peaks located at lower angle, $2\theta = 12$ and 22.0°, indicate the presence of structures with limited intercalation and can be attributed to the formation of nanocomposites (Mayouf et al. 2015). The sharp peak at $2\theta = 20.2°$ for the composites as observed might be due to the fact that the peak overlapped with the peaks for CML–2T and CML–3T, since both of the peaks appeared at the same diffraction angle. Nevertheless, the peak at $2\theta = 25.0°$ totally disappeared with the addition of TEOS in the polymer. As illustrated for T1, T2 and T3 (Fig. 5), the entire CML–T composites were almost fully intercalated in the matrix. The dispersion and intercalation of the composites could be observed in the SEM micrographs. Significantly, the change in visual appearance and structure of the silicate resulted in the formation of craters and voids. Variations in the surface hardness, bending and compressive strengths of these samples might be explained by the degree of densification of silica particles on the lignin surface. The diffraction peaks showed a considerable line broadening due to the crystallinity or crystalline size. The results further supported the observation of SEM that the nanocomposites thus synthesized were small particles in the nano size range. The observed high diffraction intensity at the low diffraction angle of $2\theta < 10°$ and a halo at $2\theta = 15–35°$ are known as XRD characteristics, peculiar to crystalline SiO_2 with silanol (Si–OH) groups, described as SiO_2·xH2O (Hanid et al. 2014). The structural change of silicate (from amorphous SiO_2·xH_2O to crystalline SiO_2) leading to the release of water of crystallization may produce craters at the surfaces and voids in the bulks. The increase in the concentration of TEOS may lead to thermal shrinkage. The variations in the surface

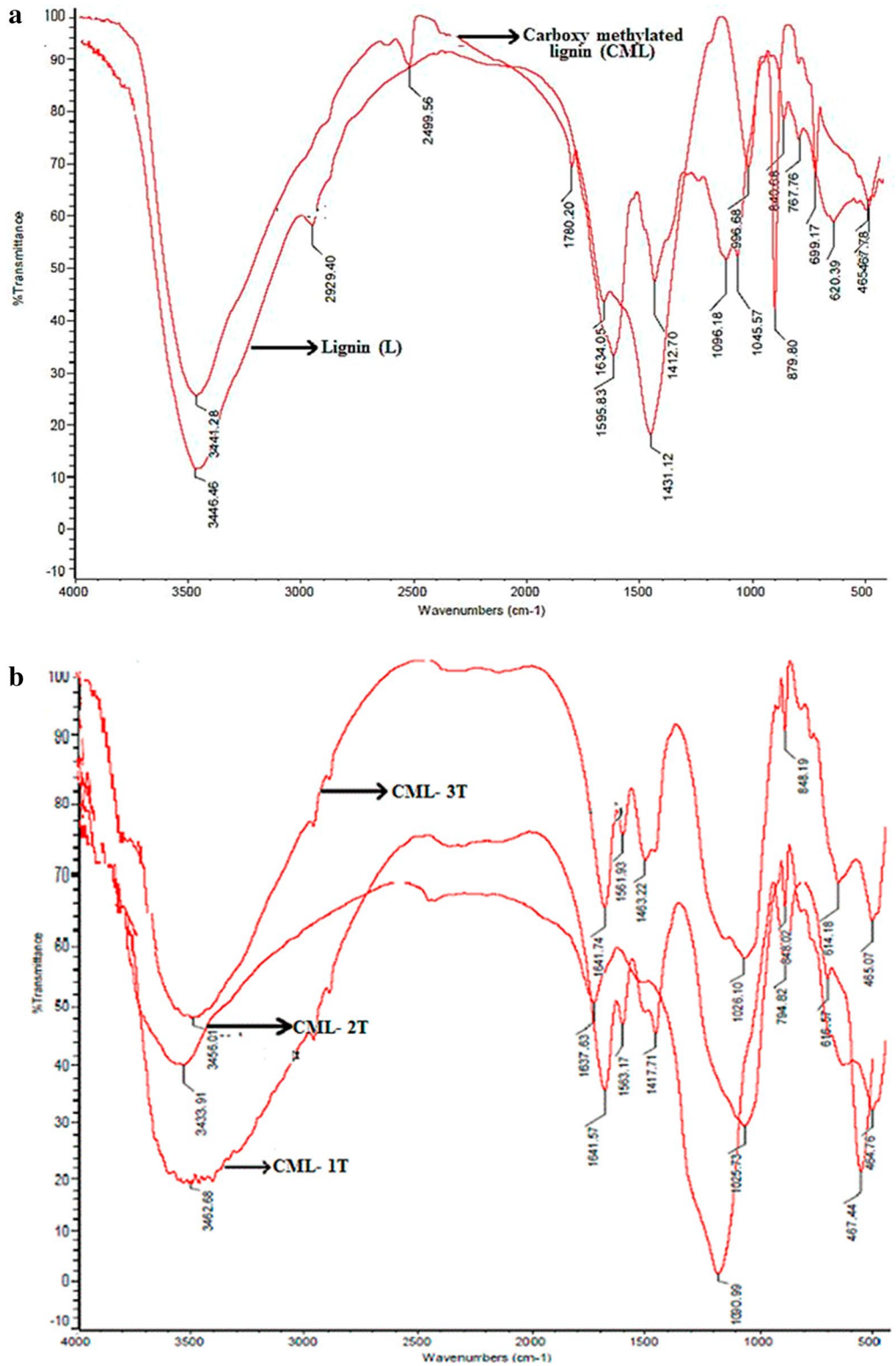

Fig. 2 **a** FT-IR spectra of lignin extracted from rice straw (RS) and carboxymethylated lignin (CML). **b** FT-IR spectra of synthesized CML–1T, CML–2T and CML–3T composites

Table 2 Peak positions of various modes of vibration in the FT-IR spectra of lignin, carboxymethylated lignin and CML–T composites during sol–gel reaction

Chemical bond	Chemical structure	Wavenumbers (cm^{-1})
C–C stretch	Aromatic ring	1595.83 cm^{-1}
C–C stretch	Aromatic ring	1412.70 cm^{-1}
C–stretch	Carbonyl group	1096.18
=C–H	Alkenes	699 and 767
–C≡C–H or C–H bend	Different functional groups of lignin	620
C–H stretch	Alkanes	2929.40
O–H stretch	Phenolic group and carboxyl	3500
C=O stretch	Carboxylic acid	1780
–C=C– stretch	Alkenes	1634.05
–C=C–	Alkenes	1634.05
C–C stretch	Aromatic ring	1431.12
–	Carboxyl ring	1412.70
=C–H bend and O–H bend	Carboxyl ring	800 and 996
O–H stretch		3441
–C=C– stretch	Alkenes	1641.74
C–C stretch	Aromatics group	1561.93
C–H bend	Alkanes	1453.22
C–H group	Aromatic ring	849.19
=C–H bend	Alkenes	849.19
O–H stretch	Phenolic group and carboxyl	3456.01

hardness and the bending and compressive strengths of these samples might be explained by the degree of densification. The X-ray diffraction pattern (Fig. 5) of CML–T composites revealed strong broad peaks of nanosilica centred in the range of 22–23° (2θ), which is in agreement with the strong broad peak characteristic of crystalline silicate-based composites (Mayouf et al. 2015). The diffraction peaks were in accordance with the hexagonal phase of barium having lattice constants $a = 5.53912$ Å and $c = 4.958$ Å. On the basis of the above studies, crystallinity indices, porosity and grain sizes of the CML–T nanocomposites have been calculated using Eqs. (1), (2) and (3) and presented in Table 3.

Electrical conductivity, turbidity and effect of nanocomposites on organic matter

The electrical properties of composites are influenced by the electronic structure of the atoms within the molecules (bonding type, bandgaps, etc.) and by the size and shape of the particles. Since electronic properties change with reduction in particle size to nanoscopic dimensions, the bandgaps and distance between adjacent levels within electron energy bands alter the chemical reaction. In the present study, composites are composed of nanoscopic particles; therefore, a larger percentage of the atoms in the mass get exposed to the material and alter the electrical conductivity of lignosulphonate, TEOS and nanocomposites at RT (Table 4).

Specific surface area and pore diameter measurement indicated that the surface area of the composite was high. Therefore, the higher fraction of mesopores contributed to the high degree of adsorption capacity. Previous reports reveal that the turbidity is caused by the presence of particles and coloured material in water. The change in colour of composites with the increasing concentration of TEOS (Fig. 1) may be attributed to the high concentration of particles.

The present study provides evidence that the CML–T composites affect the behaviour of soil properties, which are specially influenced by pH, temperature, electrical conductivity and total dissolved solids (TDS). pH values indicate the high alkaline nature of the soil in the presence of lignin, TEOS and CML–T composites. TDS induces a higher presence of CML–T composites in soil suspensions, thus suggesting a possible transport through the circulating soil solution. Table 5 summarizes the properties of soil studied in the presence of lignin, TEOS and CML–T composites.

The estimation of protein (by Lowry's method), carbohydrate (by anthrone test) and lipid content, respectively, for CML–1T, CML–2T and CML–3T and control samples were found to be as follows: protein = 26.1 ± 0.21, 29.12 ± 0.23, 22.06 ± 0.26 and 10.36 ± 0.22 mg/mL, carbohydrate = 22.38 ± 0.12, 26.18 ± 0.21, 13.69 ± 0.01 and 12.89 ± 0.11 mg/mL, and lipid = 32.91 ± 0.03, 29.63 ± 0.22, 43.49 ± 0.24 and 23.69 ± 0.19 mg/mL (Sadasivam and Manickam 2008).

Antimicrobial activities

Inorganic antibacterial material usually in the form of a non-volatile composite is considered as safe and heat resistant, compared to organic materials. Metal ions having antibacterial and antifungal activities, such as TiO_2 and TEOS, are impregnated in a mineral or blended with a carrier to form the composite or applied as a coating (Prabhu and Poulose 2012). Appropriate release of antibacterial silanol ions from the composite can effectively inhibit the growth of harmful microbes. As the ions are taken up by the microbes, they react and bind to the cellular enzyme and inhibit enzyme activity and multiplication of microbes, thus killing the microbes (Shameli et al. 2012). The CML–T (10 and 20 µL) composites were tested for their antimicrobial activity against *P. aeruginosa, E. coli, S. aureus and B. subtilis*. A clearance zone of inhibition could be observed on the surface of the medium containing the bacterial cultures except in *E. coli*. Table 6 confirms that the lignin-based composites

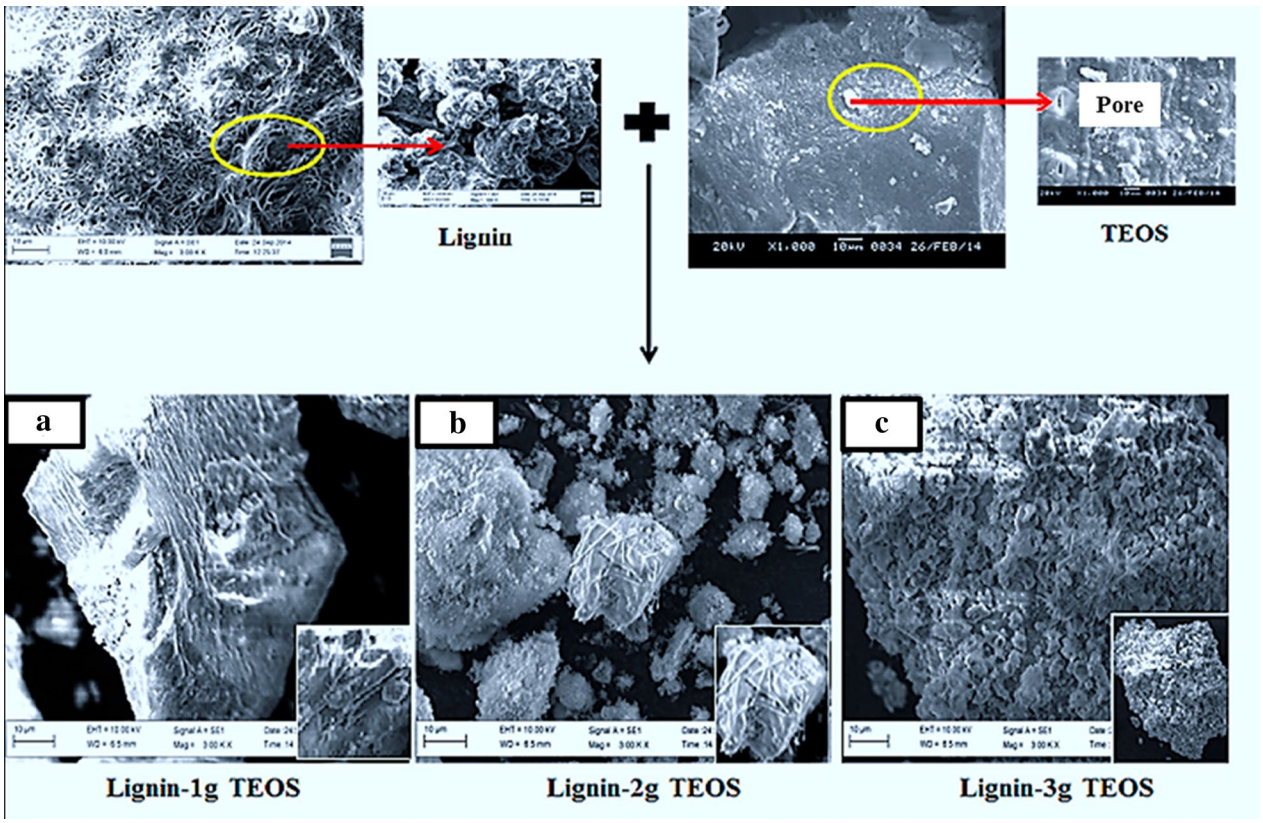

Fig. 3 Scanning electron micrographs (SEM) of carboxymethylated nanocomposites (CML–T): **a** CML–1T, **b** CML–2T and **c** CML–3T

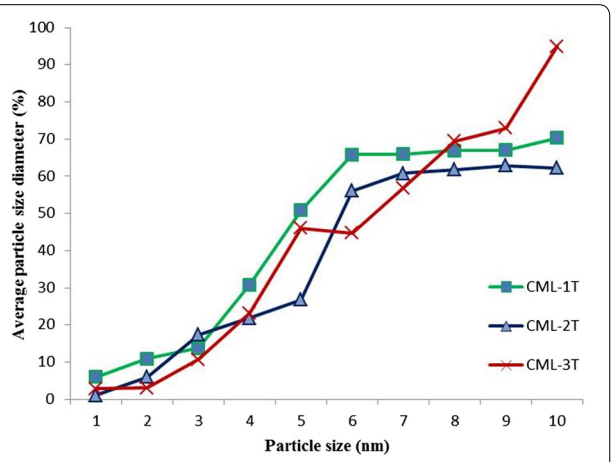

Fig. 4 Particle size distribution (PSD) curves of the CML–T composites (CML–1T, CML–2T, CML–3T) at median range (D_{50})

(CML–T) have broad-spectrum antimicrobial activity. It is well known that lignin itself has shown antimicrobial activity due to its cationic property. Therefore, the antibacterial CML–T composites are proposed to be used as packaging materials to protect valuable stuffs from bacterial contamination. Additionally, it may be applied in the preparation of biofilters or biological membranes for wastewater treatment from industrial effluents.

One of the plausible reasons of antibacterial activities of CML–Ts could be their nanoscale size and larger surface area of pathogen, due to which they could easily reach the nuclear content of bacteria (Shameli et al. 2012). In the polymeric matrix, some researcher reported that silicate ions released from the surface of the composite are responsible for their antibacterial activity (Uppuluri et al. 2015). Their mode of antimicrobial action may be related to their ability to inactivate microbial adhesions, enzymes, cell envelope transport proteins, etc. due to their complexation with polysaccharides (Cowan 1999). Lignin is also a known antibacterial agent and tends to inhibit the growth of a wide spectrum of microorganisms and, therefore, may lead to synergistic increase in the antimicrobial activity as one of the components of CML–T composites (Jesionowski et al. 2015).

Adsorption kinetics of CML–T nanocomposites

The effect of biosorbent doses on the adsorption of Ni (II) and Cd (II) ions was evaluated in the range of 0, 20, 40 and 60 mg/L, and the initial metal concentration for

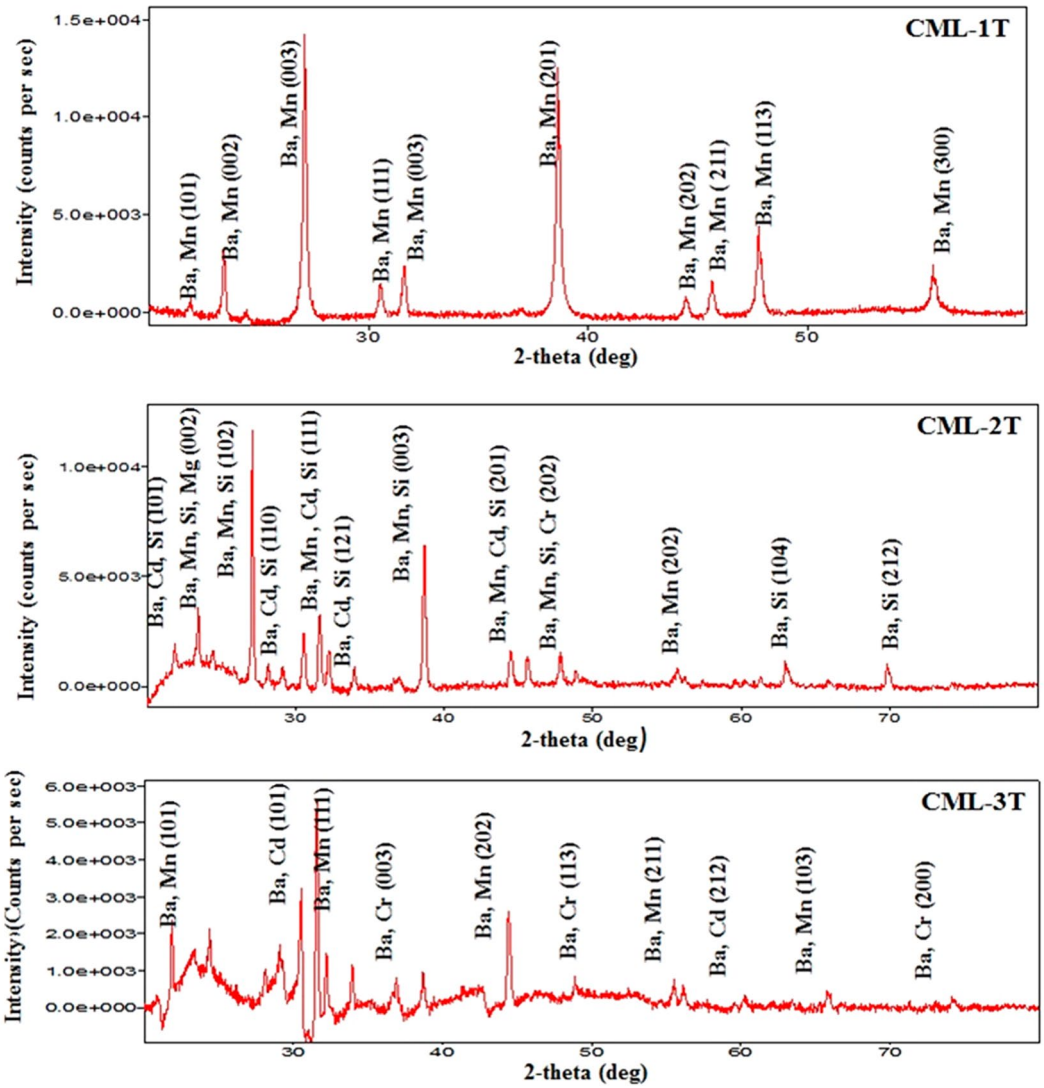

Fig. 5 X-ray diffraction (XRD) spectra of CML–1T, CML–2T and CML–3T composites

Table 3 Crystallinity indices, porosity and grain size of the CML–T nanocomposites

Sample	Crystallinity (%)	Porosity (%)	Grain size (nm)
CML–1T	63.82	51.34	355
CML–2T	46.10	24.65	560
CML–3T	61.42	39.16	160

Table 4 Study of electrical conductivity of lignosulphonate, TEOS and nanocomposites

Sample name	Electrical conductivity
Mili Q water	0.76
TEOS	1.00
Lignosulphonate	0.92
CML–1T	0.71
CML–2T	0.94
CML–3T	0.82

both metals was fixed at 25 mg/L. For Ni (II), the highest and lowest adsorption recorded was 70.72 ± 2.5 and 16.83 ± 0.6 %, respectively, at biosorbent doses of 60 and 20 mg/L, respectively (Ni, CML–3T), Fig. 6a, and for Cd (II) ions, the highest and lowest adsorption was 81.79 ± 3.5 and 20.19 ± 1.5 %, respectively, for biosorbent dose of 40 mg/L (Cd, CML–2T) Fig. 6b. Increase in the percentage of the metal adsorption with adsorbent

Table 5 Effects (pH, temperature, electronic conductivity and total dissolved solids) of nanocomposites on organic component (soil)

Sample name (Conc. mg/ml)	pH	Temperature (in °C)	Electronic conductivity and its temperature (°C)	Total dissolved solids (TDS) and its temperature (°C)
Soil sample (control)	*7.787*	*35.2*	*249.4 µS (36.3)*	*539.8 ppm (37.1)*
25 mg CML	8.318	34.4	0.806 µS (41.4)	164.5 ppm (37.2)
50 mg CML	8.356	34.67	0.801 µS (41.1)	171.9 ppm (37.8)
75 mg CML	9.102	34.89	0.721 µS (41.2)	193.2 ppm (37.7)
100 mg CML	9.114	34.21	0.711 µS (40.9)	216.6 ppm (38.1)
25 mg T	11.874	35.6	6.125 µS (36.5)	3.688 ppt (37.3)
50 mg T	11.998	35.71	6.098 µS (36.4)	4.198 ppt (37.9)
75 mg T	11.901	35.44	6.006 µS (35.2)	4.200 ppt (38.1)
100 mg T	11.892	35.98	5.890 µS (35.7)	4.319 ppt (38.9)
25 mg CML–1T	8.027	36.1	434.8 µS (36.5)	281.6 ppm (37.3)
50 mg CML–1T	8.367	36.12	433.9 µS (36.4)	293.7 ppm (37.8)
75 mg CML–1T	8.449	36.78	465 .7 µS (36.1)	280.6 ppm (38.1)
100 mg CML–1T	8.312	36.63	446.1 µS (36.6)	288.9 ppm (38.8)
25 mg CML–2T	7.669	35.23	248.5 µS (36.2)	153.0 ppm (37.2)
50 mg CML–2T	7.778	35.21	248.1 µS (36.2)	159.4 ppm (36.1)
75 mg CML–2T	7.918	35.29	244.2 µS (35.1)	167.9 ppm (37.9)
100 mg CML–2T	8.910	35.48	241.8 µS (34.8)	181.9 ppm (37.8)
25 mg CML–3T	7.556	37.10	524.4 µS (31.0)	317.4 ppm (37.3)
50 mg CML–3T	7.664	37.40	517.1 µS (30.9)	321.3 ppm (38.2)
75 mg CML–3T	7.898	37.89	514.9 µS (30.4)	333.9 ppm (38.8)
100 mg CML–3T	7.913	37.56	512.0 µS (30.1)	345.8 ppm (39.1)

Table 6 Antimicrobial activity of CML–T nanocomposite against Gram-positive and Gram-negative bacteria: a comparative study for size of clearance zone as observed by the well diffusion method

Sample concentration (mg/µl)	Bacterial strains			
	P. aeruginosa **(MTCC 741) (mm)**	***S. aureus*** **(MTCC 96) (mm)**	***E. coli*** **(MTCC 739)**	***B. subtilis*** **(MTCC 441) (mm)**
Control				
10	Nil	Nil	Nil	Nil
20	1.3	2.0	Nil	3.0
CML–1T				
10	0.9	2.2	Nil	4.0
20	0.89	2.1	Nil	0.3
CML–2T				
10	0.69	1.9	Nil	0.21
20	0.55	1.61	Nil	0.19
CML–3T				
10	0.52	0.21	Nil	0.16
20	0.42	0.29	Nil	0.12

doses could be attributed to increase in the adsorbent surface areas, augmenting the number of adsorption sites available, as reported earlier (Cardoso et al. 2011). On the other hand, increase in the adsorbent dose promotes decrease in the amount of metal uptake per gram of adsorbent (q), (Fig. 6a, b), an effect that can be mathematically explained by combining Eqs. (4) and (5). This result suggests that a large adsorbent dose reduces the unsaturation of the adsorption sites and likewise the number of such sites per unit mass decreases, resulting in

a relatively much reduced adsorption at higher adsorbent doses.

The effect of shaking time on the adsorption of Ni (II) and Cd (II) ions by CML–T (25 mg/mL) (Fig. 7a, b). More than 50 % adsorption occurred after 48 h. However, for a complete uptake under the given condition, 96 h shaking appeared to be necessary. Therefore, all adsorption studies were monitored under shake condition up to 4 days at an interval of 24 h for both the metal ions.

The adsorption behaviour of CML–T for various metal ions is reported as percent adsorption of metal ions, plotted against equilibrium pH. The effect of pH on adsorption of Ni (II) and Cd (II) ions is shown in Fig. 8a, b. A similar trend of increase in percent adsorption with increasing pH was observed in acidic pH 5.0 for the two metals ions. As the metal ions exist as cationic species at pH < 5.0 (Cardoso et al. 2011), the result directly supports the cation exchange mechanism (Fig. 9). Therefore, at these pH values, adsorption would show effective mechanism to remove the metal ions from the aqueous solution. There are several reasons for introducing new functional groups of lignin and silica on the surface of nanocomposites. The most important is to increase the binding sites, to change the pH range for metal sorption as well as to vary the sorption sites and the uptake of metal ions, to increase adsorption selectivity for the target metal ions. A recent report shows 48 h as optimum for achieving 89 % metal absorption (Vinu et al. 2014).

Our findings clearly suggest that the most efficient biosorbent hybrid for Ni (II) was CML–3T, as it showed the highest level of rough surface with approximately 75 % adsorption at pH 5.0 within 96 h, and for Cd (II) CML–2T was the best biosorbent as it showed 81.79 ± 4.6 % metal adsorption at pH 5.0 in 72 h. This could be possibly because of the crystalline and porous structures of CML–T nanocomposites suitable for biosorption for cationic metal ions at different concentrations.

Mechanism

The surface of the lignocellulosic polymers may be modified through various chemical treatments, such as carboxymethylation to enhance the binding sites by increasing the functional groups on the surface of lignin. This process makes the surface negatively charged and promotes the formation of stable suspension from CML to nanosize. A high concentration of TEOS or too low pH causes a rapid agglomeration of the modified lignin. Thus, our results conclude that the pH range and the concentration of TEOS were the two key factors to obtain the optimum reaction condition. Mechanisms of the sorption include physical adsorption, hydrogen bonding, electrostatic interaction and acidic–basic interaction. Strong electrostatic (i.e. ion dipole) interactions are expected to take place between the –OH ions of hydrolysed silica and the electron-rich oxygen atoms (Robert et al. 2010). Moreover, FT-IR peak at 1595 cm^{-1} confirmed the carboxymethylation of extracted lignin. Additionally, SEM images displayed high agglomeration and lower diameter of lignin (Fig. 3a–e). The SEM micrographs of freeze-dried CML–T nanocomposites (Fig. 3e) showed a coherent system of lignin–TEOS based composites, with overall diameters <100 nm. The morphological analysis of the composites exhibited a diminution in sol aggregates by increasing TEOS concentration, which consequently shows higher degree of crystallinity in SEM

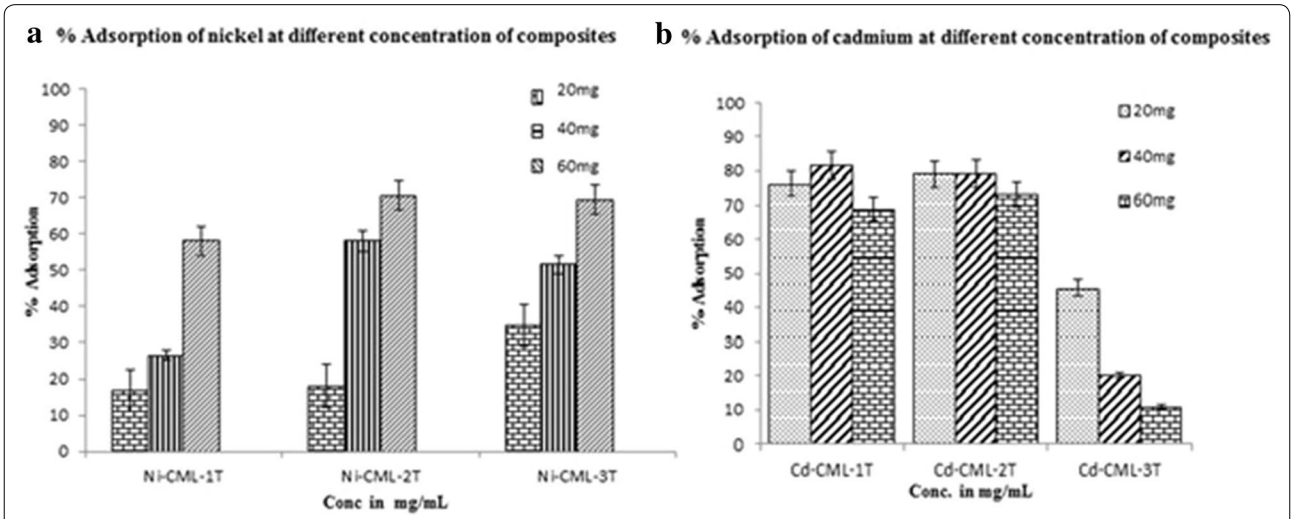

Fig. 6 Percent adsorption of **a** Ni (II) and **b** Cd (II) at different concentrations (0, 20, 40, 60 mg/L) of CML–T composites

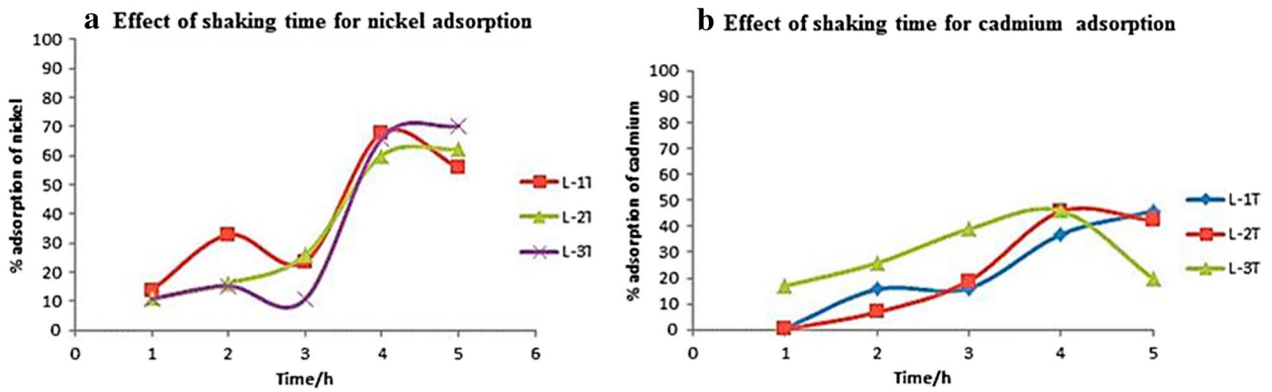

Fig. 7 Percent adsorption of **a** Ni (II) and **b** Cd (II) at different shaking times (0, 24, 48, 72 and 96 h) by CML–T composites (25 mg/mL)

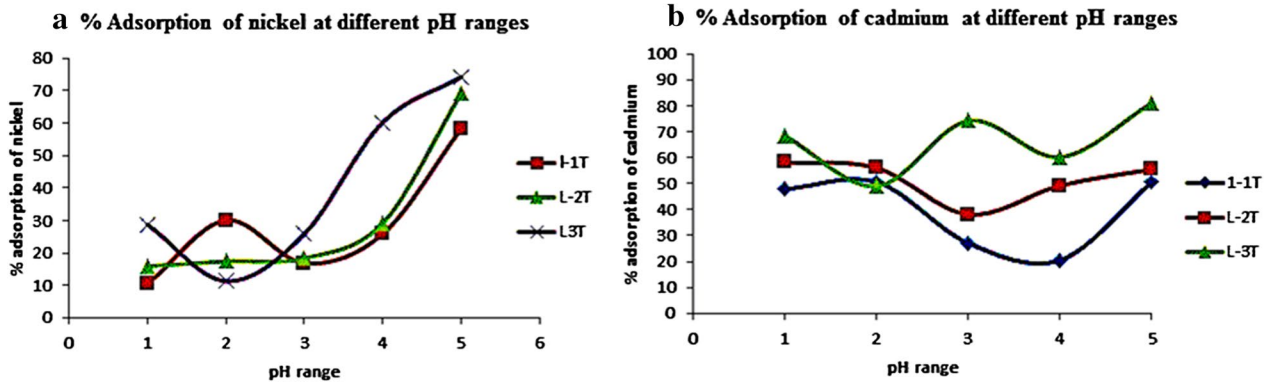

Fig. 8 Percent adsorption of **a** Ni (II) and **b** Cd (II) at different pH values (1.0, 2.0, 3.0, 4.0 and 5.0) by CML–T composites (25 mg/mL)

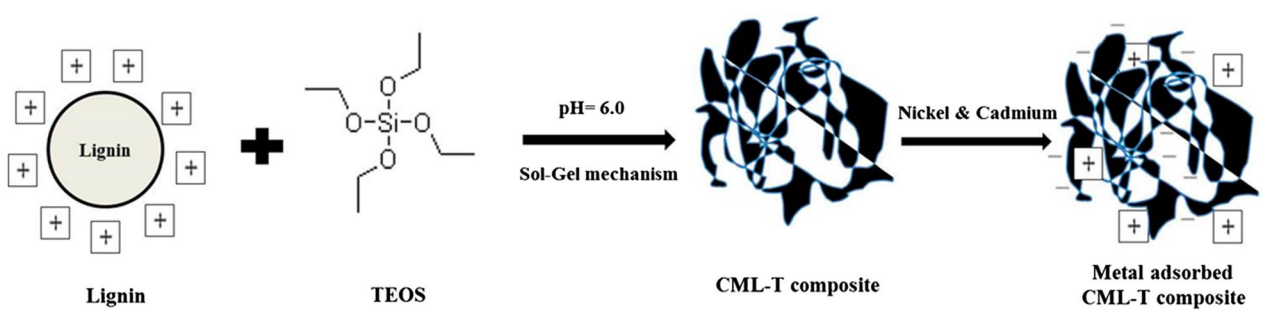

Fig. 9 The proposed mechanism of adsorption of Ni (II) and Cd (II) ions by CML–T composite as the adsorbent. The *circle* stands for the metals with negative charges

micrographs (Khalil et al. 2014). The crystalline composites further demonstrate increase in adsorption of metal ions. Based on our findings as well as the principle of cation exchange, a schematic representation to explain the mode of action of CML–T for application in removal or reduction in the toxicity of metals present in effluents has been presented in Fig. 10.

Regeneration and disposal of adsorption materials

The biocomposite is biodegradable in nature. It is economical, but a fresh stock is required for every batch of chelation. The composite and metal bound as well as unbound to it becomes non-toxic (Fig. 11) through reduction of toxic metal ions into non-toxic ionic form and can be disposed as landfilling and composting by

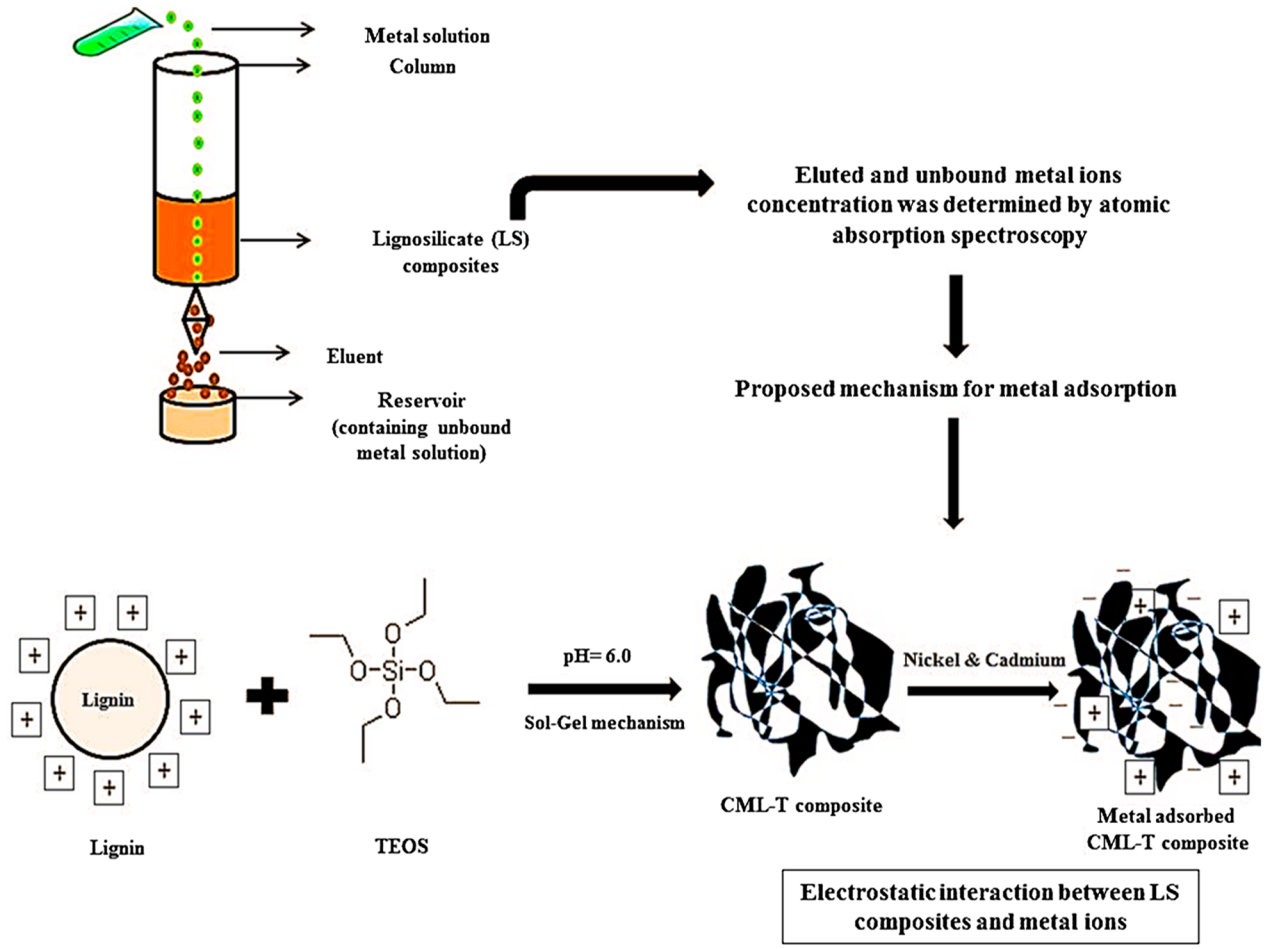

Fig. 10 Schematic representation of metal ion adsorption by crystalline CML–T composite

natural bio-geo chemical cycle (Li et al. 2010). Heavy metals can be immobilized or aggregated by microbial hypha during composting. Their existing formations can be changed by materials such as lime, which are added to compost materials (Chen et al. 2010).

Conclusion

In the present study, RS-based lignin and TEOS composite (CML–T composites) proved to be a good adsorbent of heavy metal ions (cadmium and nickel) from wastewater. The presence of hydroxyl (–OH) and methyl groups ($–CH_3$) in the CML–T nanocomposites provided binding sites for the metal ions. The maximum metal removal (81.79 %) is obtained at 72 h of contact time and at pH value of 5.0, which is at par with any synthetic adsorbent. It can be thus considered as a viable alternative to activated carbon, ion exchange resin and other synthetic adsorbents used for this purpose. Modification of the –OH groups of lignin through carboxymethylation and synthesis of composite from the modified lignin are important for the reaction parameters. The hybrid is thermally stable and its metal sorption capacity is strongly influenced by the crystalline and porous structure of the adsorbent, rather than the composition and quantity of dispersed superficial functional groups. The composites also possess antibacterial property and are proposed to be used as packaging materials to protect valuable stuffs from bacterial contamination. The results therefore suggest a potential application of nanotechnology in the development of natural biopolymer-based biodegradable materials like biofilters for wastewater treatment by removal or reduction in the toxicity of metals present in effluents. This will increase the availability of co-products suitable for producing various chemicals, thus reducing our dependence on non-renewable energy sources.

The results emphasize that it is beneficial to extract lignin using agro-wastes (RS) to produce value-added products which minimize the environmental pollutions created by otherwise unmanageable agricultural wastes.

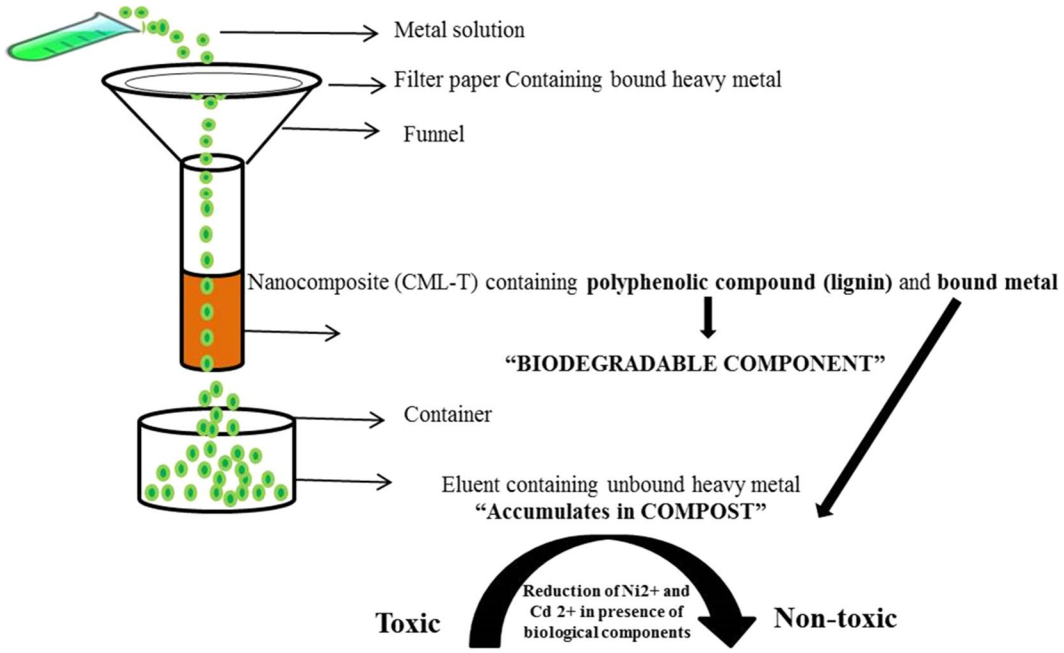

Fig. 11 Schematic representation of the proposed disposal method of the biodegradable composite

Application of the modified lignin in combination with TEOS could be furthered for the production of advanced biodegradable, eco-friendly biomaterials with tailored properties for making biofilters or biomembranes, which could be utilized for removal of several other environmental pollutants or eliminating the chance of bacterial contaminants.

Abbreviations

TEOS: tetra-ethoxy silane; RS: rice straw; CML–T: carboxymethylated lignin–TEOS; PSD: particle size determination; SEM: scanning electron microscopy; XRD: X-ray diffraction.

Authors' contributions

HJ provided the concept of study, designed experimental plan and contributed to analysis and inference of results whereas KS contributed through execution and optimization of experiments along with analysis of data and manuscript preparation. All authors read and approved the final manuscript.

Acknowledgements

The authors wish to thank the Department of Biotechnology, Government of India for financial support under the DBT-BUILDER Project (No. DBT/BT/PR7020/INF/22/177/12). DST-INSPIRE Senior Research Fellowship (DST Registration No. IF110479) to one of us (KS) by the Department of Science & Technology (DST), Ministry of Science & Technology, Government of India is thankfully acknowledged. Technical support from national facilities at STIC, Cochin (India), for FT-IR analysis, National Institute of Immunology (NII), Delhi, for particle size analysis and the National Institute of Technology (NIT), Raipur, for XRD analysis is acknowledged. The Head of Department, Department of Biotechnology is gratefully acknowledged for his moral support during the work.

Competing interests

The authors declare that they have no competing interests.

Funding

"This work was supported by the Department of Science & Technology (DST) and Department of Biotechnology, Ministry of Science & Technology, Government of India, in the form of DST-INSPIRE Senior Research Fellowship [DST Registration No. IF110479] to one of us (KS)" and DBT-BUILDER (Sanction Order No. DBT/BT/PR7020/INF/22/177/12) Grant, respectively.

Received: 16 February 2016 Accepted: 26 May 2016
Published online: 13 June 2016

References

Alexander L, Klug HP (1949) and (1950) Determination of crystallite size with the X-ray spectrometer. J Appl Phys 21 and 137

Atwood JL, Lehn JM (1996) Comprehensive Supramolecular Chemistry. Pergamon Press, Oxford

Cardoso NF, Lima EC, Pinto IS, Amavisca CV, Royer B, Pinto RB, Alencar WS, Pereira SFP (2011) Application of cupuassu shell as biosorbent for the removal of textile dyes from aqueous solution. J Environ Manag 92:1237–1247

Chen G, Zeng G, Du C, Huang D, Tang L, Wang L, Shen G (2010) Transfer of heavy metals from compost to red soil and groundwater under simulated rainfall conditions. J Hazard Mater 181:211–216

Cowan MM (1999) Plant Products as Antimicrobial Agents. Clin Microbiol Rev 12(4):564–582 **(PMCID: PMC88925)**

Gao GM, Zou HF, Liu DR, Miao LN, Juan JG, Gan SC (2009) Influence of surfactant surface coverage and aging time on physical properties of silica nanoparticles. Colloids Surf A: Physicochem Eng Aspects 350:33–37

Gardebjer S, Bergstrand A, Larsson A (2014) A mechanistic approach to explain the relation between increased dispersion of surface modified cellulose nanocrystals and final porosity in biodegradable films. Eur Polym J 57:160–168

Gomes ME, Reis RL (2004) Biodegradable polymers and composites in biomedical applications: from catgut to tissue engineering Part 1 available systems and their properties. Int Mater Rev 49(5):261–273

Gulyas H, Argaez ASO, Kong F, Jorge CL, Eggers S, Otterpohl R (2013) Combining activated carbon adsorption with heterogeneous photocatalytic

oxidation: lack of synergy for biologically treated greywater and tetraethylene glycol dimethyl ether. Environ Technol 34(11):1393–1403
Gupta GK, De S, Franco A, Balu AM, Luque R (2016) Sustainable biomaterials: current trends, challenges and applications. Molecules 21(48):1–11
Hanid NA, Wahit MU, Guo Q, Mahmoodian S, Soheilmoghaddam M (2014) Development of regenerated cellulose/halloysites nanocomposites via ionic liquids. Carbohydr Polym 99:91–97
Harish BS, Uppuluri KB, Anbazhagan V (2015) Synthesis of fibrinolytic active silver nanoparticle using wheat bran xylan as a reducing and stabilizing agent. Carbohydr Polym 132:104–110
Heidari A, Younesi H, Mehraban Z, Heikkinen H (2013) Selective adsorption of Pb(II), Cd (II), and Ni (II) ions from aqueous solution using chitosan–MAA nanoparticles. Int J Biol Macromol 61:251–263
Ichkitidze L, Podgaetsky V, Selishchev S, Blagov E, Galperin V, Shaman Y, Pavlov A, Kitsyuk E (2013) Electrically-conductive composite nanomaterial with multi-walled carbon nanotube. Mater Sci Appl 4:1–7
In: Sparks DL (Ed.) SSSA Book Series. Methods in soil analysis, part 3: Chemical Methods, Soil Science Society of America, Inc., Madison. 1996
Jimenez LHV, Pavlick A, Mendez JRR (2013) Chemical characterization of raw and treated agave bagasse and its potential as adsorbent of metal cations from water. Ind Crop Prod 43:200–206
Khalil HPSA, Davoudpour Y, Islam MN, Mustapha A, Sudesh K, Dungani R, Jawaid M (2014) Production and modification of nanofibrillated cellulose using various mechanical processes. Carbohydr Polym 99:649–665
Kim JY, Hwang H, Oh S, Kim YS, Kim UJ, Choi W (2014) Investigation of structural modification and thermal characteristics of lignin after heat treatment. Int J Biol Macromol 66:57–65
Klapiszewski L, Rzemieniecki T, Krawczyk M, Malina D, Norman M, Zdarta J, Majchrzak I, Dobrowolska A, Czaczyk K, Jesionowski T (2015) Kraft lignin/silica-AgNPs as a functional material with antibacterial activity. Coll Surf B Biointerfaces. 134:220–228
Kumagaia S, Matsuo Y (2013) Composite produced from rice husk and chopped carbon fiber without using any binders. Ind Crop Prod 43:640–647
Kumar S, Saha T, Sharma S (2015) Treatment of pulp and paper mill effluents using novel biodegradable polymeric flocculants based on anionic polysaccharides: a new way to treat the waste water. Int Res J Eng Technol 2(4):1–14
Li F, Shungui Z, Zhuang L, Tao L, Li X, Wu C, Liu T (2010) Biogeochemical interactions between Fe(II)/(III) species cycles and transformation of reducible substrates in subtropical soils. 19th World Congress of Soil Science, Soil Solutions for a Changing World, 23–26 (Published in DVD)
Li SM, Jia N, Ma MG, Zhang Z, Liu QH, Sun RC (2011) Cellulose-silver nanocomposites: microwave-assisted synthesis, characterization, their thermal stability, and antimicrobial property. Carbohydr Polym 86:441–447
Malarvizhi GL, Chandran P, Retnakumari AP, Ramachandran R, Gupta N, Nair S, Koyakutty MA (2014) Rationally designed photo-chemo core shell nanomedicine for inhibiting the migration of metastatic breast cancer cells followed by photodynamic killing. Nanomed Nanotech Biol Med 10:579–587
Maniglia BC, Domingos JR, de Paula RL, Blacido DRT (2014) Development of bioactive edible film from turmeric dye solvent extraction residue. LWT-Food Sci Technol 56:269–277
Mayoufi A, Nsib MF, Ahmed O, Houas A (2015) Synthesis, characterization and photocatalytic performance of W, N, S-tri-doped TiO_2 under visible light irradiation. C R Chim 18:875–882
Min T, Jiali W, Duncan MD, Robert MA, Aicheng C (2010) A novel approach for lignin modification and degradation. Electrochem Commun 12(4):527–530
Mohamed E, Hanem R, Mohamed A (2013) Biosorption and removal of Cr(VI)–Cr(III) from water by eco-friendly gelatin biosorbent. J Environ Chem Eng 2(1):1–8
Mohdy FAA, Abdel-Halim ES, Ayana YMA, Sawy SME (2009) Rice straw as a new resource for some beneficial uses. Carbohydr Polym 75:44–51
Nair V, Panigrahy A, Vinu R (2014) Development of novel chitosan-lignin composites for adsorption of dyes and metal ions from wastewater. Chem Eng J 254:491–502
Nardis D, Monti Natale CD, Amico AD, Siciliano P, Forleo A, Epifani M, Taurino A, Rella R, Paolesse R (2004) Preparation and characterization of cobalt porphyrin modified tin dioxide films for sensor applications. Sensor Actuat B 103(1):339–343
Nassar MA, Youssef AM (2012) Mechanical and antibacterial properties of recycled carton paper coated by PS/Ag nanocomposites for packaging. Carbohydr Polym 89:269–274
Parajuli D, Inoue K, Ohto K, Oshima T, Murota A, Funaoka M, Makino K (2005) Adsorption of heavy metals on crosslinked lignocatechol: a modified lignin gel. React Funct Polym 62(2):129–139
Paul DR, Robeson LM (2008) Polymer nanotechnology: Nanocomposites. Polymer 49(15):3187–3204
Prabhu S, Poulose EK (2012) Silver nanoparticles: mechanism of antimicrobial action synthesis, medical applications, and toxicity effects. Int Nano Lett 2(32):1–10
Sadasivam S, Manickam A (2008) Biochemical methods, 3rd edition, New Age International (P) Ltd. New Delhi
Salem NM, Awwad AMJ (2011) Biosorption of Ni(II) from electroplating wastewater by modified (*Eriobotrya japonica*) loquat bark. Saudi Chem Soc 18(5):379–386. doi:10.1016/j.jscs.2011.07.008
Sciban M, Kukic D, Klasnja M, Beszedes S, Prodanovic J (2014) Adsorption capacities of different lignocellulosic materials for copper ions. Bull Eng ISSN 2067–3809:1–4
Segal L, Creely JJ, Martin AE, Conrad CM (1959) An empirical method for estimating the degree of crystallinity of native cellulose using the X-ray diffractometer. J Text Res 29:786–794
Shameli K, Ahmad MB, Jazayeri SD, Shabanzadeh P, Sangpour P, Jahangirian H, Gharayebi Y (2012) Investigation of antibacterial properties silver nanoparticles prepared via green method. Chem Cent J 6(73):1–10
Shilin L, Qiufang Y, Dandan T, Tengfei Y, Xiaoya L (2012) Highly flexible magnetic composite aerogels prepared by using cellulose nanofibril networks as templates. Carbohydr Polym 89:551–557
Shweta K, Jha H (2015) Rice husk extracted lignin–TEOS biocomposites: effects of acetylation and silane surface treatments for application in nickel removal. Biotechnol Rep 7:95–106
Slavutskya AM, Bertuzzi MA (2014) Water barrier properties of starch film reinforced with cellulose nanocrystals obtained from sugarcane bagasse. Carbohydr Polym 110:53–61
Stober W, Fink A, Bohn E (1968) Controlled growth of monodisperse silica spheres in the micron size range. J Colloid Interface Sci 26:62–69
Taha AA, Wu Y, Wang H, Li FJ (2012) Preparation and application of functionalized cellulose acetate/silica composite nanofibrous membrane via electrospinning for Cr(VI) ion removal from aqueous solution. Environ Manage 112:10–16
Tantra R, Cackett A, Peck R, Gohil D, Snowden J (2012) Measurement of Redox Potential in Nanoecotoxicological Investigations. Int J Toxicol Article ID 270651:1–7
Tibolla H, Pelissari FM, Menegalli FC (2014) Cellulose nanofibers produced from banana peel by chemical and enzymatic treatment. LWT-Food Sci Technol 59:1311–1318
Weng CH, Lin YT, Hong DY, Sharma YC, Chen SC, Tripathi K (2014) Effective removal of copper ions from aqueous solution using base treated black tea waste. Ecol Eng 67:127–133
Xu J, Yang H, Fu W, Du K, Sui Y, Chen J, Zeng Y, Li M, Zou G (2007) Preparation and magnetic properties of magnetite nanoparticles by sol–gel method. J Magn Magn Mater 309(2):307–311
Yadav M, Rhee KY, Park SJ (2014) Synthesis and characterization of graphene oxide/carboxymethylcellulose/alginate composite blend films. Carbohydr Polym 110:18–25
Yang D, Wu X, Qiu X, Chang Y, Lou H (2014) Polymerization reactivity of sulfomethylated alkali lignin modified with horseradish peroxidase. Bioresour Technol 155:418–421
Yumei QY, Tian B, Zou J, Zhang Y, Zheng L, Wang LY, Chunguang R, Wang Z (2010) A novel mesoporous lignin/silica hybrid from rice husk produced by a sol-gel method. Bioresour Technol 101:8402–8405
Zhang P, Qiao A, Jia G, Wang CC (2013) Synthesis of mesoporous magnetic Co-NPs/carbon nanocomposites and their adsorption property for methyl orange from aqueous solution. J Colloid Interf Sci 389:10–15